

The structural evolution of sheath folds: A case study from Cap de Creus

G.I. Alsop^{a,*}, J. Carreras^b

^a School of Geography and Geosciences, University of St. Andrews, Scotland KY16 9AL, UK

^b Departament de Geologia, Universitat Autònoma de Barcelona, 08193 Bellaterra (Barcelona), Spain

Received 6 March 2007; received in revised form 31 August 2007; accepted 5 September 2007

Available online 2 October 2007

Abstract

It has long been recognised that within zones of intense non-coaxial deformation, fold hinges may rotate progressively towards the transport direction ultimately resulting in highly curvilinear sheath folds. However, there is a surprising lack of detailed and systematic field analysis of such “evolving” sheath folds. This case study therefore focuses on the sequential development of cm-scale curvilinear folds in the greenschist-facies El Llimac shear zone, Cap de Creus, Spain. This simple shear-dominated dextral shear zone displays superb three dimensional exposures of sheath folds defined by mylonitic quartz bands within phyllonite. Increasing amounts of fold hinge curvature (δ) are marked by hinge segments rotating into sub-parallelism with the mineral lineation (Lm), whilst the acute angle between the axial-planar hinge girdle and foliation (ω) also displays a sequential reduction. Although Lm bisects the noses of sheath folds, it is also clearly folded and wrapped-around the sheath hinges. Lm typically preserves a larger angle (θ) with the fold hinge on the lower limb (L) compared to the upper (U) limb ($\theta_L > \theta_U$), suggesting that Lm failed to achieve a steady orientation on the lower limb. Adjacent sheath fold hinges forming fold pairs may display the same sense of hinge arcing to define *synthetic curvature*, or alternatively opposing directions of *antithetic curvature*. Such patterns reflect original buckle fold geometries coupled with the direction of shearing. The ratio of long/short fold limbs decreases with increasing hinge curvilinearity, indicating sheath folds developed via stretching of the short limb, rather than migrating or rolling hinge models. This study unequivocally demonstrates that *both* hinges of fold pairs become curvilinear with sheaths closing in the transport direction recording greater hinge-line curvilinearity compared to adjacent return hinges. This may provide a useful guide to bulk shear sense.

© 2007 Elsevier Ltd. All rights reserved.

Keywords: Shear zones; Sheath folds; Fold evolution; Cap de Creus

1. Introduction

Sheath folds, which may most simply be defined as folds displaying more than 90° of hinge-line curvature, are generated in a wide variety of materials and deformation regimes including constriction and general shear (see Jiang and Williams, 1999; Alsop et al., 2007). However, by far the most commonly recorded setting involves non-coaxial deformation dominated by simple shear (see Alsop and Holdsworth, 2006 for a review). An explanation for sheath fold development that has

dominated thinking for over a quarter of a century involves simple shear-dominated deformation being perturbed by an initial deflection which becomes increasingly non-cylindrical during passive amplification (Cobbold and Quinquis, 1980). Perturbations in flow can be generated from a number of sources and create curvilinear folds as demonstrated via field work (e.g. Fossen and Rykkelid, 1990), modelling studies (e.g. Marques and Cobbold, 1995; Bons and Urai, 1996; Rosas et al., 2002), and combinations of these (see review by Mandal et al., 2004).

Although the experimentally-derived model of Cobbold and Quinquis (1980) has gained near universal acceptance “almost to the point where it is used unquestioningly as *the* explanation” (Skjerna, 1989 p. 690), there has in reality been very

* Corresponding author.

E-mail address: gia@st-andrews.ac.uk (G.I. Alsop).

little detailed analysis of natural sheath fold systems to test or refine the model. In many cases, sheath fold pairs are portrayed as displaying a single curvilinear hinge-line whilst the “return” hinge is shown as being relatively cylindrical or even omitted. Clearly, if such relationships are correct then they have major implications on the use of “drag” folds and curvilinear folds as kinematic indicators (e.g. see recent debate in Williams et al., 2006; Kuiper et al., 2007). This work represents the first study to systematically measure a suite of geometric parameters around curvilinear folds and sheath folds. In addition, the geometry of sheath fold pairs which close in opposing directions about the transport direction are carefully examined. Variations in the curvilinearity of hinge-lines forming such fold pairs test the validity of employing sheath folds as kinematic indicators.

2. Geological setting of “El Llimac” shear zone

For the purpose of our case study, a 60 m long segment of the greenschist-facies Llimac shear zone covering $\sim 100 \text{ m}^2$ in Cala Prona, northern Cap de Creus shear belt has been investigated (Fig. 1a,b). We have carefully chosen this particular shear zone as it satisfies the following considerations: a) The regional setting of this individual shear zone, which belongs to an anastomosing network of shears, is well known (e.g. Carreras and Santanach, 1973; Carreras and Casas, 1987; Carreras, 1997, 2001; Carreras et al., 1977, 2005). b) The shear zone is well exposed and geometrically well defined as it cuts across schists at high angles with both margins of the shear zone clearly exposed. c) Superb differential weathering of folds by wave and aeolian activity enables intricate and detailed relationships to be directly observed and measured in three dimensions. d) The geometrical analysis of shear zones performed by Carreras (1997, 2001) demonstrates that the Cap de Creus shears (including those in the study area) display only slight departures from ideal simple shear deformation. Although limited deviations from simple shear occur at the margins of shear zones, increasing shear strain towards the centre of the shear zones results in the foliation becoming sub-parallel to the shear plane, and the deformation approaching simple shear. Thus deformation within the internal portions of the Cap de Creus shear zones (where sheath folds develop) can be approximated to simple shear-dominated.

The (D_3) Llimac shear zone is a moderately NE-dipping and NW-SE trending zone marked by dextral shearing which cuts across medium grade schists bearing an ENE trending sub-vertical foliation (Fig. 1b). This pre-existing composite (S_1 – S_2) foliation is defined by the preferred orientation of micas parallel to axial planes and thinned limbs of isoclinal F_2 folds. The 2–6 m wide Llimac shear zone displays 150 m dextral displacement which allows a bulk mean shear strain (γ) of 30 to be deduced. However the presence of lozenges with reworked but partially preserved F_2 folds indicates that strain is highly inhomogeneous, with $\gamma > 10$ at the inner margins of the shear zone (see Carreras, 1997). This intense deformation causes nodular quartz segregations to be transformed into thin (mm-cm) quartz bands or ribbons. Pre-existing

F_2 folds are completely transposed and obliterated by the effects of high D_3 shear strain, with the formation of a new mylonitic foliation (S_m) (Fig. 1c). Within quartz-mylonites, a gently NW-plunging lineation (L_m) is also well defined within the plane of S_m (Fig. 1d). This is a stretching lineation defined by mineral elongation in quartz, but also by stretching of the initially irregular interface of quartz and schists which becomes a corrugated intersection lineation. The mylonitic (D_3) quartz bands are extensively folded with more than 600 minor sheath fold hinges measured in the case study area.

3. Geometry of sheath folds – a descriptive framework

A variety of parameters associated with curvilinear folds may be measured and calculated as illustrated on Fig. 2. The amount of fold hinge-line curvature (δ) represents the supplement to the apical angle (β), with the interlimb angle (α) forming the acute angle between the two fold limbs (Fig. 2) (see Alsop and Holdsworth, 2006). The angle (θ) between the fold hinge and the lineation (L_m) representing linear datum, together with the angle (ω) between axial plane and mylonitic foliation (S_m) representing planar datum can also be calculated (Fig. 2). The fold limb ratio is defined as long limb length/short limb length, whilst the axial planar layer thickness is the width of the folded mylonitic quartz band measured along the axial plane (Fig. 2).

F_3 folds in the case study area display variable hinge orientations and hinge-line curvature with respect to the shear direction, which is considered to parallel the mineral elongation lineation in zones of intense simple shear deformation. The fold hinges ($N = 623$) collectively define a well-developed stereographic fold hinge girdle which extends over an arc of 180° and parallels the associated mean axial plane (Fig. 1e,f). For the purposes of structural analysis, curvilinear folds are simply categorised into either North- or South-closing structures which are typically bisected by the NNW trending mineral lineation (L_m). In addition, North- or South-closing curvilinear folds can be further subdivided into “S” or “Z” shaped segments when viewed down plunge (Fig. 3). Minor folds associated with North- and South-closing hinges display broadly similar stereographic girdle patterns sub-parallel to mean axial plane orientations (Fig. 3a–d). In detail however, the orientation of S and Z fold segments reverses from North- to South-closing hinges (Fig. 3a,b). Thus, in North-closing structures, Z folds trend anticlockwise (–ve) of L_m , whilst S fold segments are clockwise (Fig. 3e,f). The converse holds true for South-closing folds. This distinct pattern is considered a geometric consequence of folds displaying different senses of clockwise or anticlockwise obliquity to L_m , and subsequently rotating in opposing senses towards the shear direction during progressive deformation.

The extreme variability of fold hinge orientations results in distinctive patterns on plots comparing fold plunge and trend, and angles of hinge pitch (or rake) (Fig. 4a,b). Such consistent trends indicate that the mylonitic foliation (S_m) which is closely parallel to the X-Y surface, and the mineral lineation (L_m) which lies sub-parallel the X-direction of the finite strain

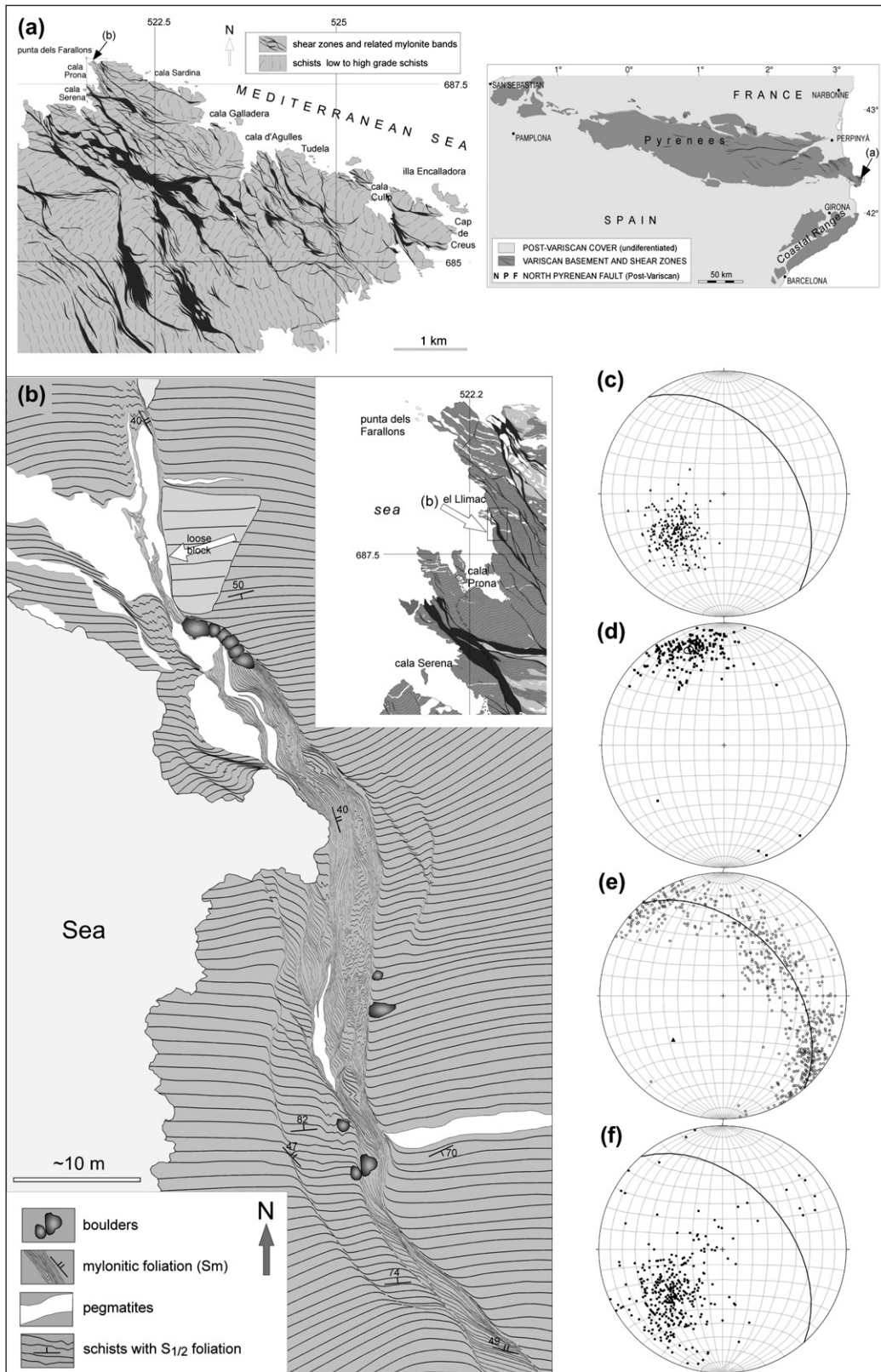


Fig. 1. a) The Northern Cap de Creus shear belt and inset showing location within the Pyrenees. b) Detailed map of the case study segment of the “El Llimac” shear zone (map drawn on an aerial photograph and contains some minor topographic distortions). c) Stereoplot of mylonitic foliation (Sm). Great circle defines mean foliation (142/43E) ($N = 220$). d) Stereoplot of mylonitic stretching lineation (Lm). Circled area shows mean Lm (17/340) ($N = 223$). e) Stereoplot of fold hinges. Best-fit great circle (triangle shows pole) to fold hinges also shown (139/45E) ($N = 623$). f) Stereoplot of fold axial planes. Great circle defines mean axial plane (139/46E) ($N = 386$). All data collected from the case study area (b).

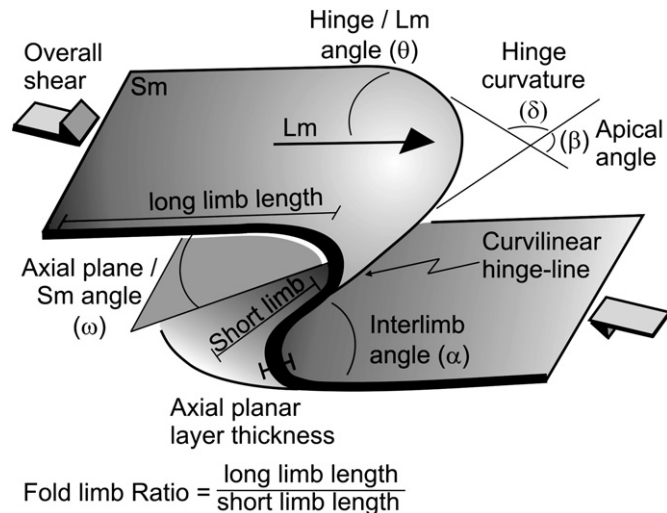


Fig. 2. Diagram illustrating the parameters that may be measured around sheath folds, together with calculations concerning fold limb ratios.

ellipsoid form consistent reference “datum” about which folding displays extreme variability. Thus, despite S_m and L_m being locally folded around the minor folds, they typically maintain their relationship to the finite strain ellipsoid during progressive deformation.

The consistent sense of S and Z fold obliquity about L_m in North or South-closing structures indicates that no larger-scale sheath axial surfaces have been crossed (see Alsop and Holdsworth, 1999, 2002, 2007). However, closer examination of S and Z fold patterns reveals an asymmetric distribution about L_m , with North-closing Z fold segments and South-closing S folds being preserved closer to L_m (Fig. 3a,b,e,f). This skewed pattern is highlighted on Fig. 4c where the obliquity of S and Z fold segments from individual curvilinear folds are directly compared. The amount of asymmetry about L_m varies as a function of overall fold hinge curvature (δ), and typically increases until fold curvature reaches 90° (Fig. 4d). Greater levels of hinge curvilinearity ($\delta > 90^\circ$) result in lower levels of asymmetry as both hinge segments defining the sheath sequentially rotate towards sub-parallelism with L_m (Fig. 4d). Such asymmetry of fold obliquity about L_m may be interpreted in terms of fold hinge-line vergence, where curvilinear hinges verge towards larger scale culminations (see Alsop and Holdsworth, 1999, 2004a,b).

4. Analysis of curvilinear folds and sheath folds

Folds in the Llimac shear zone develop in thin (mm-cm) bands of quartz-mylonite hosted in a phyllonitic (mylonitic schist) matrix. Importantly, the previously mylonitised layers display consistent contrasts in competence (quartz and phyllonite) and similar sub-parallel orientation with respect to the shear zone. All folded quartz ribbons exhibit the same microfabric patterns (Carreras et al., 1977; Carreras and Garcia-Celma, 1982) indicating that folds developed during a continuous shearing process with no change in deformation conditions or bulk shear direction. It is assumed that the

variety of observed curvilinear fold shapes form a continuous spectrum that reflects structures preserved at different stages along their evolutionary path. For descriptive purposes a broad threefold division is established, with each stage considered to represent a different phase of fold evolution.

4.1. Stage 1 “Initial fold stage”

Stage 1 or the “Initial fold stage” includes folds that exhibit cylindrical or only mildly curved hinges displaying $<30^\circ$ of hinge-line curvature (δ) (Figs. 5a and 6a–d). These folds are considered to be representative of the early or juvenile stages of the evolutionary sequence, with fold pairs frequently marked by close antiforms and complimentary synformal return hinges displaying extremely cusped geometries (Fig. 6c,d). Stage 1 folds display hinges at high angles with the shear direction (mean θ 67°), fold axial planes and associated hinge-girdle planes that are markedly inclined to the foliation (mean ω 35°), together with close-tight interlimb angles (mean α 30°) (Fig. 5a). Folds with only slightly curving hinge lines ($\delta < 20^\circ$) display hinges at even higher angles to the shear direction (θ 85°), greater axial plane/foliation obliquities (ω 40°) and close interlimb angles (α 44°). The limb ratio of these folds also display greater values (3.6) when compared to Stage 1 folds as a whole as does mean axial planar thickness. These variations are considered to reflect the evolutionary path and development of Stage 1 fold geometries during initial stages of progressive shearing. Open folds (mean interlimb angles of 90°) with axial planes developed at high angles to the foliation (ω 64°) and hinges within 30° of the shear direction (marked by L_m) form a very minor ($<4\%$) component of Stage 1 folds. In addition, we record no close folds with hinges lying within 30° of the shear direction. Our data therefore indicate that within this case study, Stage 1 folds initiate at high angles ($\theta > 85^\circ$) to the shear direction.

4.2. Stage 2 “Curvilinear fold stage”

Stage 2 or the “Curvilinear fold stage” includes folds displaying 30° – 90° of hinge-line curvature. These mature folds display hinges at moderate angles with the shear direction (mean θ 57°), fold axial planes and the associated hinge-girdle planes that are gently inclined to the foliation (mean ω 17°), together with tight interlimb angles (mean α 17°) (Figs. 5b and 6e–h). Mean limb ratios (2.4) and axial planar thicknesses (mean 6.5 mm) continue to show reductions when compared with Stage 1 folds (Fig. 5a,b). It should be noted that some curvilinear hinge-lines associated with both Stage 1 and Stage 2 folds are not bisected by the mylonitic lineation (L_m) marking the shear direction. Both measured segments of the curved fold hinge therefore display the same sense of obliquity to L_m , and hence will undergo the same sense of axial rotation towards the shear direction. Thus, with increasing deformation, such folds are destined to evolve into sub-cylindrical hinge-lines subparallel to L_m , rather than highly curved ($\delta > 90^\circ$) sheath folds. Indeed, all folds displaying $>90^\circ$ of hinge curvature in the present study are bisected by L_m .

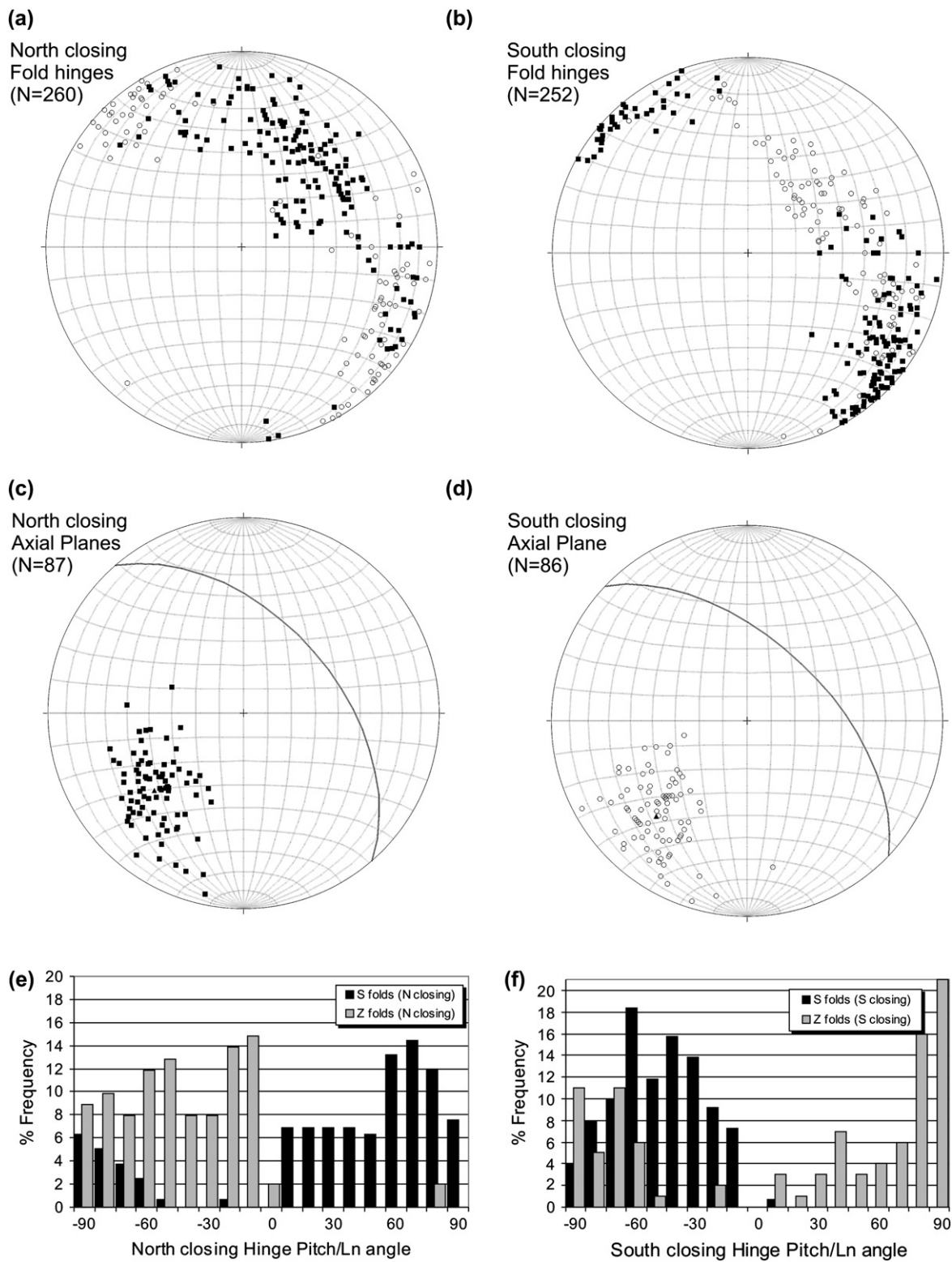


Fig. 3. a) Stereoplots of fold data collected from the case study area (see Fig. 1b) with North-closing fold hinges ($N = 260$) divided into S (solid squares) and Z (open circles) fold hinges. b) Stereoplot of South-closing fold hinges ($N = 252$) divided into S (solid squares) and Z (open circles) fold hinges. c) Stereoplot of North-closing fold axial planes (mean great circle $139/51^E$, $N = 87$). d) Stereoplot of South-closing fold axial planes (mean great circle $134/57^E$, $N = 86$). e, f) % Frequency distribution histograms of fold hinge pitches relative to the adjacent mineral lineation Lm (0 datum). Due to the gently-plunging nature of Lm, structural relationships are best described in terms of angle of pitch (or rake) relative to Lm. Fold hinges may pitch clockwise (+ve) or anticlockwise (-ve) relative to Lm, and are divided into S (black) and Z (tone) hinges for North-closing folds (e) and South-closing folds (f).

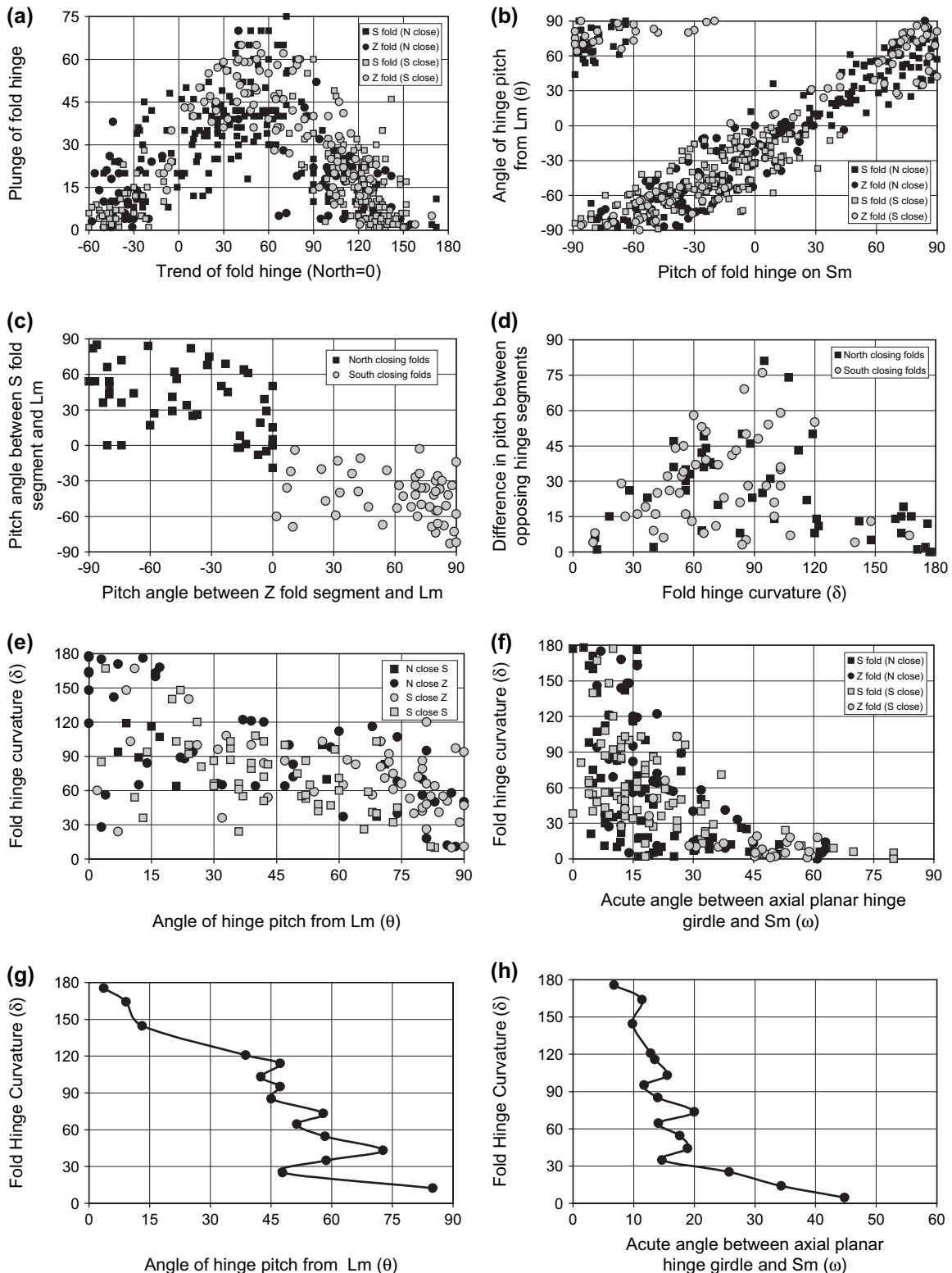


Fig. 4. Plots of fold and fabric relationships with North-closing hinges (black) and South-closing hinges (grey) subdivided into *S* folds (squares) and *Z* folds (circles). Fold hinges develop clockwise (+ve) or anticlockwise (–ve) of the adjacent mineral lineation (Lm). a) Trend of fold hinge plotted against plunge of fold hinge displays a systematic pattern with NW-plunging folds plotted as –ve values in order to show the continuation of geometric trends. The steepest plunges (75°) are directed towards the ENE directly down the dip of the foliation surface. b) Pitch of fold hinge plotted against angle (θ) of fold hinge pitch from Lm. c) Angle of hinge pitch between *S/Z* fold segments and Lm are directly plotted against each other for *individual* curvilinear folds. d) Plot comparing amount of fold hinge curvature (δ) against the difference in pitch values of opposing hinge segments. e) Plot comparing the angle (θ) of hinge pitch from Lm and fold hinge curvature (δ). f) Plot comparing the acute angle (ω) between the axial planar hinge girdle and mylonitic foliation (Sm) with fold hinge curvature (δ). g, h) Summary plots of e) and f) respectively with mean values calculated for each 10° division of fold hinge curvature.

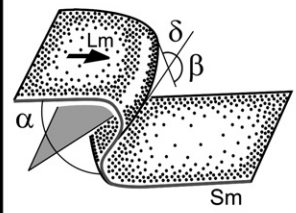
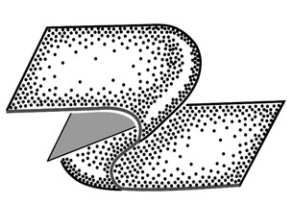
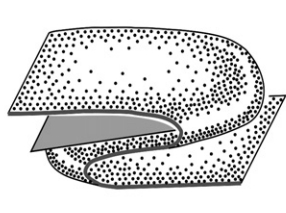
Fold Parameters	(a) Stage 1 Initial fold stage	(b) Stage 2 Curvilinear fold stage	(c) Stage 3 Evolved fold stage
Fold style			
Hinge curvature (δ)	Low (0–30°)	Moderate (30°–90°)	High (90°–180°)
Apical angle (β)	High (150°–180°)	Moderate (150°–90°)	Low (0°–90°)
Inter-limb angles (α)	Open-close folds 30° (45° where $\delta < 20^\circ$)	Tight folds Mean 17°	Sub-isoclinal folds 11° (7° where $\delta > 160^\circ$)
Hinge-Lm angles (θ)	High (>60°) mean 67°	Moderate (60°–45°) 57°	Low (<45°) mean 29°
Axial Plane - Sm Angles (ω)	High (>30°) mean 35°	Moderate (30°–15°) 17°	Low (<15°) mean 11°
Fold limb ratio	High (mean 3.64)	Moderate (mean 2.47)	Low (mean 2.1)
Axial planar thickness	High (mean >7.5mm)	Moderate (mean 6.5mm)	Low (mean <6mm)

Fig. 5. Schematic sketches and calculated mean data for fold parameters associated with a) initial ($N = 157$), b) curvilinear ($N = 110$), and c) evolved ($N = 50$) fold stages. Relationships of fold hinges to the transport lineation (Lm) and mylonitic foliation (Sm) are also provided. Interlimb angles (α) and hinge curvature (δ) display a progressive reduction through the Initial – Curvilinear – Evolved (ICE) sequence.

4.3. Stage 3 “Evolved fold stage”

Stage 3 or the “Evolved fold stage” includes extreme folds displaying 90°–180° of hinge-line curvature to define sheath folds. These profoundly curvilinear folds display hinges at low angles with the shear direction (mean θ 29°), fold axial planes and the associated hinge-girdle planes that are sub-parallel with the foliation (mean ω 12°), together with extremely tight interlimb angles (mean α 11°) (Figs. 5c and 7a–h). Folds with intensely curving hinge lines ($\delta > 160^\circ$) defining hairpin geometries are also marked by eye-fold closures in sectional view (Fig. 8a), and display hinges sub-parallel (θ 7°) to the shear direction, axial planes sub-parallel (ω 9°) with the foliation and sub-isoclinal (α 7°) interlimb angles. The limb ratios (1.77) and axial planar thicknesses (mean 3.5 mm) of these folds also display lower values when compared to Stage 3 folds overall (Fig. 5c). In addition, intersection or striping lineations (Sengupta and Ghosh, 2007) which form sub-parallel to fold hinges can also become curved to define hair-pin patterns (Fig. 8b).

4.4. Summary

We have described a continuum of fold shapes and geometrical relationships arising from an assumed continuous shearing. It is considered that increasing hinge-line curvature (δ) represents folds preserved at progressive stages of their

evolutionary path. Increasing δ is marked by hinge segments rotating into sub-parallelism with Lm, whilst the acute angle between the axial planar hinge girdle and foliation (ω) also displays a sequential reduction (Fig. 4e,f). These relationships reflect the rotation of (axial) planar elements towards the X-Y foliation plane, and linear (fold) elements towards the mineral lineation representing the X axis of the finite strain ellipsoid during intense non-coaxial deformation (e.g. Carreras et al., 1977; Cobbold and Quinquis, 1980; Ramsay, 1980). In detail, analysis of mean 10° intervals of fold hinge curvature reveals that the most pronounced angular reductions occur where $\delta < 30^\circ$ (Fig. 4g,h). The data are consistent with the greatest planar and linear fabric rotations occurring when fabric elements are at the highest angles to the shear plane and shear direction respectively i.e. the fabric attractors during non-coaxial deformation (Passchier, 1997; Passchier and Trouw, 2005). The systematic reduction in the fold limb ratio with increasing hinge curvilinearity reflects a relative lengthening of the short limb, consistent with its stretching and attenuation during progressive shear (Fig. 5a–c). Systematic reductions in fold interlimb angles are also consistent with limb rotation during progressive shear (Fig. 5).

Thus, a broad threefold division of fold development has been established incorporating Initial (0°–30° hinge curvature), Curvilinear (30°–90°) and Evolved (90°–180°) fold stages (I-C-E). The variety of observed fold geometries from

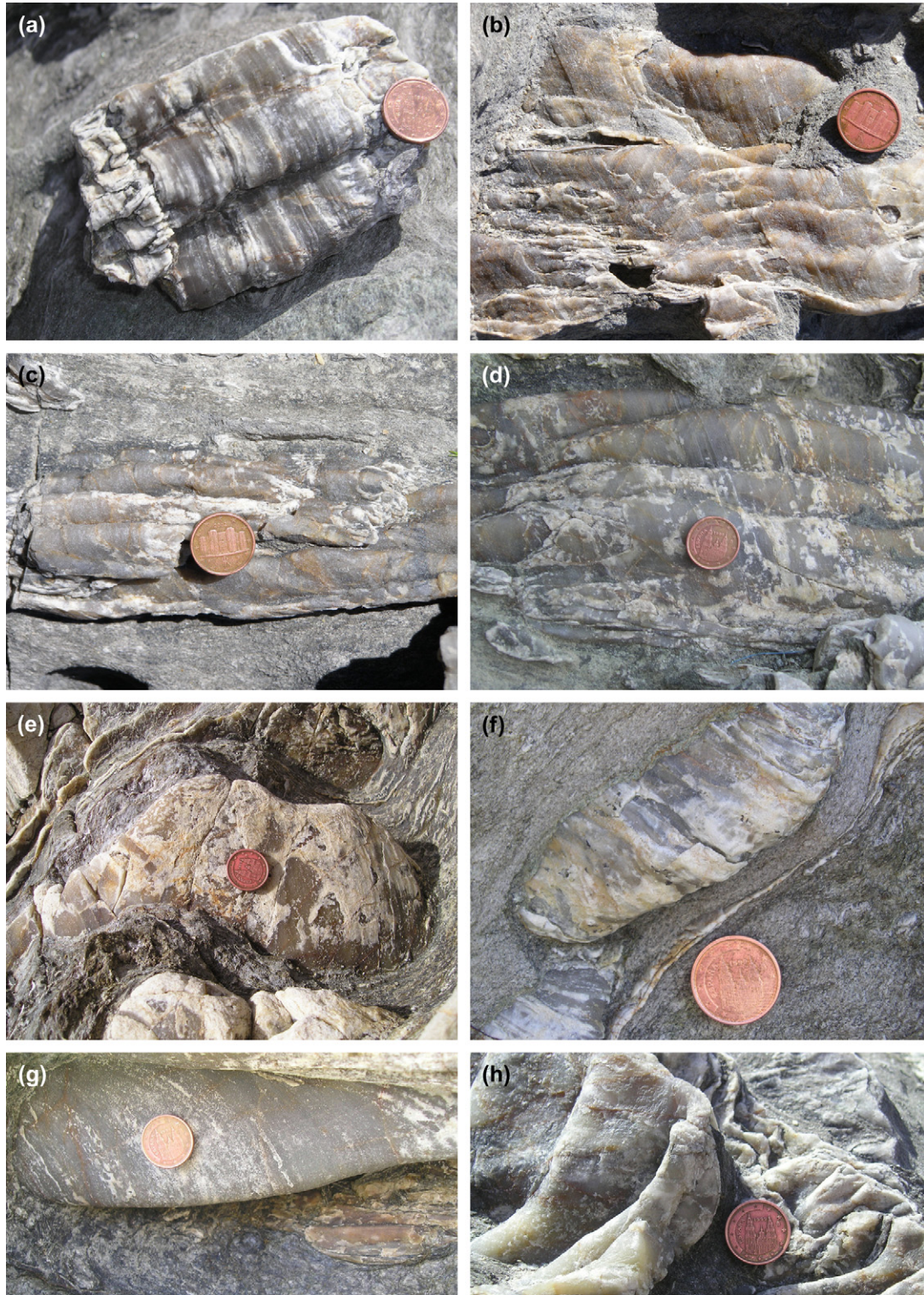


Fig. 6. Photos of folded quartz mylonite layers within the phyllonitic host of the case study area, El Llimac shear zone (see Fig. 1 for location). Coin is 15 mm diameter in each case. a)–d) show Stage 1 “Initial folds” with mildly curvilinear hinges ($<30^\circ$ curvature) developed at high angles to the mineral lineation (Lm), which is itself clearly refolded. The hinges display open-close interlimb angles, with rounded antiformal closures separated by pinched synforms to define overall cusped geometries. e)–h) show Stage 2 “Curvilinear folds” with moderately (30° – 90°) curving hinges and tight interlimb angles. The mineral lineation (Lm) typically bisects the acute angle between the curved fold hinge segments and is again clearly refolded.

sub-cylindrical to intensely curvilinear sheaths may simply reflect structures preserved or “frozen” at different stages within ICE along their particular evolutionary route. Continuing shear sometimes leads to a second generation Stage 1 fold

overprinting an older, previously formed, Stage 3 fold. This results in locally complex evolutionary sequences marked by fold interference as suggested elsewhere (e.g. Ghosh and Sengupta, 1984; Sengupta and Ghosh, 1997). Whilst local

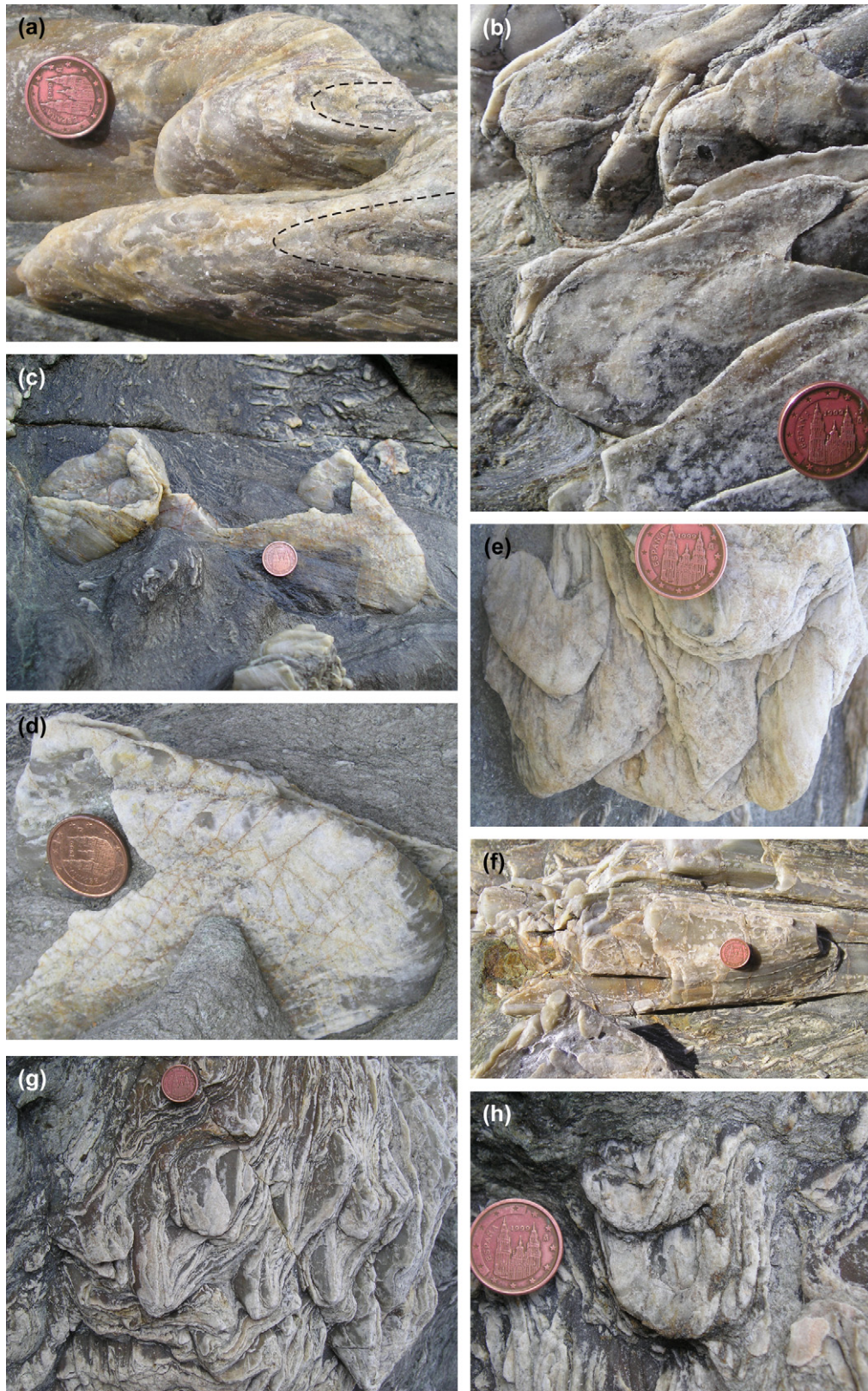


Fig. 7. Photos of intensely folded quartz mylonite layers within the phyllonitic host of the El Llimac shear zone. Coin is 15 mm diameter in each case. a)–h) show Stage 3 “Evolved folds” with highly curvilinear hinges ($>90^\circ$ curvature) bisected by the mineral lineation (Lm). Dashed line in a) marks “hair pin” intersection lineations which parallel fold hinge. These sheath folds display tight to sub-isoclinal interlimb angles with one direction of fold closure dominating over the pinched return hinges. In c), adjacent sheath folds closing in opposing directions are clearly observed.

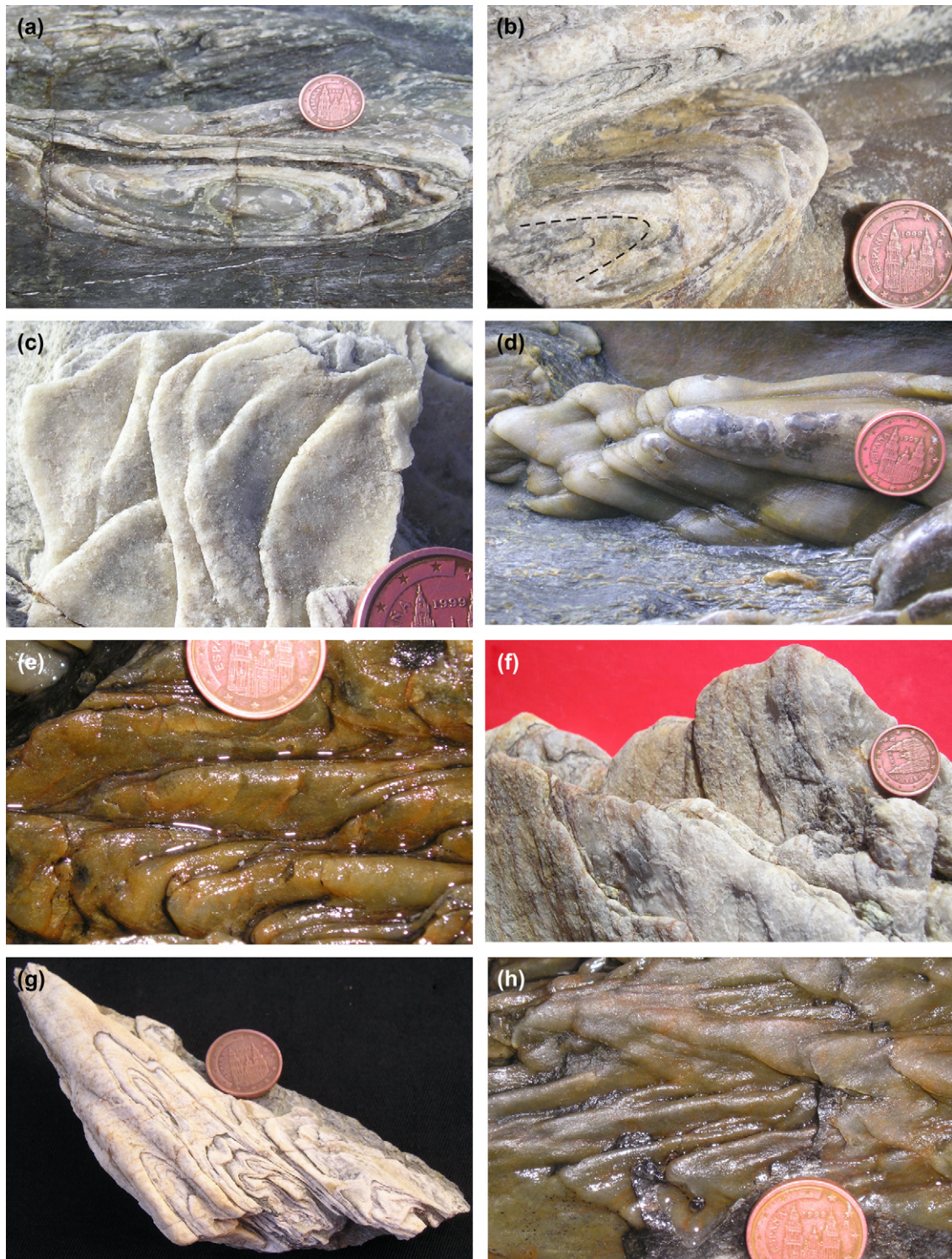


Fig. 8. Photos of intensely folded quartz mylonite layers within the phyllonitic host of the case study area, El Llimac shear zone. Coin is 15 mm diameter in each case. The photos illustrate the nature of complex fold hinge geometries. a) Eye-fold representing a y - z cross section through a highly curvilinear sheath fold displaying a curved axial plane. The closure also displays an elliptical ratio (outer-most elliptical value/inner-most elliptical value) termed R' of 0.745 to define a cats-eye-fold pattern consistent with sheath folds developed during simple shear-dominated deformation (see Alsop and Holdsworth, 2006 for details of technique). b) Plan view of a sheath fold displaying $>160^\circ$ of hinge-line curvature within a quartz mylonite layer. The lighter and darker bands (marked by dashed line) within the layer represent intersection or striping lineations that are also intensely curvilinear about and bisected by L_m . c) Bifurcating fold hinges defining variably curvilinear and sheath fold geometries. The degree of curvilinearity increases towards the left of the photo and is bisected by the horizontal L_m . d) and e) illustrate extreme asymmetry of sheath fold hinges with sheaths closing in a single direction dominating over the adjacent return hinges. Return hinges (and medial surfaces which bisect sheath folds) become pinched, resulting in "finger-like" sheaths protruding or pointing in a single direction and positioned directly on top of one another. f) Three en-echelon sheath fold hinges silhouetted against a plain background. The coin is positioned on the nearest sheath, with each off-set hinge located further from the observer and towards the left. g) Asymmetric sheath folds displaying fold hinge-line vergence away from the observer and towards a central culmination. h) Plan view of asymmetric minor sheath folds displaying an overall "S" shaped fold hinge-line vergence towards base of photograph.

reworking can influence initial fold geometries due to variable orientations of surfaces etc., each generation of fold will follow a broadly similar “life” cycle. Although these three stages may be representative of fold evolution elsewhere, we stress that other evolutionary paths exist (depending on angles of fold initiation) and that final fold geometries represent non-unique solutions to fold history. In order to further constrain fold history, we now describe the relationships between fold hinges and lineations.

5. Analysis of folded lineation patterns around sheath fold hinges

Lineations developed on foliation surfaces that are deformed around subsequent folds make distinct patterns when such surfaces are “unfolded” (Ghosh and Chatterjee, 1985; Ghosh and Sengupta, 1987; Sengupta and Ghosh, 1997, 2004; Ghosh et al., 1999; Srivastava, 2001; Sengupta and Koyi, 2001) (Fig. 6a,f,g). Lineation traces are considered by these authors to reflect the folding and contemporaneous recrystallisation of the lineation, together with the rotation history of fold hinge itself. The angle (θ) which the lineation (Lm) makes with the fold hinge on the upper (θU) and lower (θL) fold limbs can be measured (Fig. 9a). Lineations may be simply folded (where $\theta U = \theta L$), undergo a component of recrystallisation and reorientation with the folding (where $\theta U < \theta L$), or undergo complete recrystallisation such that $\theta U + \theta L = 180^\circ$ (Fig. 9a).

Our analysis shows that Lm displays curved or “U” shaped traces about the fold hinge, indicating that transport sub-parallel fold hinges have undergone significant rotation and that Lm was “active” and recrystallising as the folds developed (Fig. 9b) (e.g. Sengupta and Ghosh, 1997). Unfolding of lineations to generate “U” shaped patterns also reveals a degree of asymmetry, with Lm developed on the upper (long) limbs of folds typically displaying more acute angles (θU) with the fold hinge when compared with the folded lineation on the adjacent lower (short) limb (θL) (Fig. 9c). This relationship is observed across a range of hinge/Lm angles (and hence fold “stages”) and suggests a combination of folding of Lm around the fold hinge, coupled with a component of reorientation/recrystallisation of the quartz mineral lineation on the lower fold limb. The difference in hinge/Lm angles on each fold limb, with $\theta L > \theta U$, suggests that the lineation on the rotated lower fold limb has failed to achieve a new steady orientation, and preserves a component of higher θL values created when the fold hinge was initiated at higher angles to Lm.

Folded lineation patterns developed around culminations/depressions forming the nose of sheath folds define rectilinear patterns on an unfolded transparency (Type 1 of Ghosh and Chatterjee, 1985). However, lineation paths further along the rotated hinges of the curvilinear folds display “U” shaped traces with the sense of lineation curvature reversing across the sheath nose (Fig. 10) (e.g. Ghosh et al., 1999; Srivastava, 2001). Folded lineations may theoretically display concave or convex patterns towards the sheath nose depending on the direction of fold hinge plunge and the synformal or antiformal

nature of the sheath (Fig. 10). The lineation pattern will also become more complex across curvilinear fold pairs depending on the direction of curvature of the return hinge. If the return hinge displays a synthetic sense of hinge-line curvature i.e. both fold hinges forming the fold pair arc in the same direction, then the unfolded lineation will display “U” shaped closures pointing in opposing directions along the antiformal and synformal pairs (Fig. 10a,b). Conversely, if the return hinge displays an antithetic sense of curvature, i.e. fold hinges forming the fold pair arc in opposing directions, then the unfolded lineation displays “U” shaped closures pointing in the same direction along the antiformal and synformal pairs (Fig. 10c,d). The development of antithetic or synthetic curvature to return hinges will be critically dependent on the orientation and gentle arcing of the original buckle folds. Sheath fold pairs clearly displaying antithetic curvatures are typically associated with well-developed return hinges (Fig. 7c), whilst markedly cusped geometries may encourage synthetic curvatures.

6. Discussion

This study has systematically analysed the geometry of minor folds developed exclusively within quartz mylonite layers that are orientated sub-parallel to the shear plane prior to folding. Deformation within the shear zone is simple shear-dominated (e.g. Carreras, 1997, 2001) which removes much of the inherent complications associated with more complex three-dimensional strains (e.g. Passchier et al., 1997; Jiang and Williams, 1999; Kuiper et al., 2007). Analysis of this “simplified” system with fewer variables therefore permits greater investigation of the original geometries and controls on sheath folding.

6.1. Sheath folds and original buckles

Folds in this case study display a range of preserved or final fold geometries: namely: a) variable angles between hinge girdles and foliation (ω) for any given amount of hinge curvature (δ); and b) variable inter-limb angles (α) for folds at any given angle to Lm (θ) and hinge curvature (δ).

Although bulk shear strain is considered to be broadly consistent across the study area, local (m-scale) variations can develop and influence fold initiation and evolution. However, adjacent folds displaying variability on an even smaller (cm) scale suggests that geometric rather than kinematic influences can be significant. In some cases folds may initiate across a range of orientations prior to shearing and rotation. However, the general reduction in hinge girdle and axial planar angles to Sm with increasing curvilinearity of fold hinge lines, together with the unwrapped “U”-shaped lineation traces, indicates that folds in the case study initiated at high angles to shear.

Variability in geometric patterns can also reflect original mechanical anisotropy associated with contrasts in composition and layer thickness. Folds were measured exclusively within mylonitic quartz layers developed in a phyllonitic host, thus standardising compositional contrasts. Our data display a broad correlation between mylonitic quartz layer thickness and amount of hinge curvature, with slightly thicker

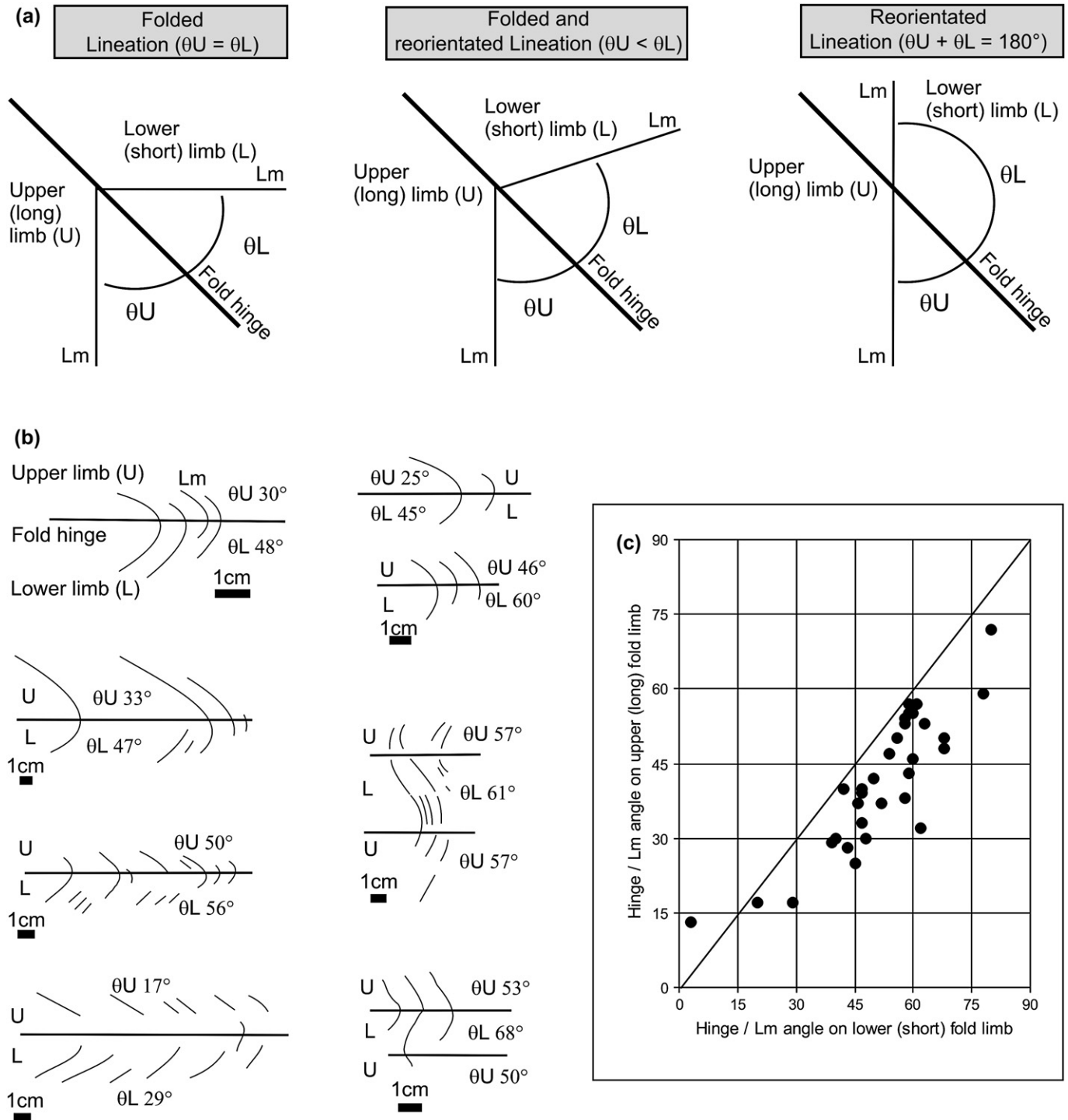


Fig. 9. a) Schematic sketches illustrating the geometric relationships between early mineral lineations (Lm) which are subsequently folded and reorientated around later oblique fold hinges. Unfolding of surfaces reveals the angular relationship (θ) between Lm and the fold hinge on both the upper (U) and lower (L) fold limbs. Three scenarios are envisaged (from left to right) in which Lm may be simply folded, both folded and reorientated via recrystallisation of minerals, or suffer complete reorientation via recrystallisation. b) Illustrations of folded lineation (Lm) patterns drawn from transparencies wrapped around folds in the case study area. Lineations display markedly curved traces from the upper (U) to the lower (L) fold limbs indicating significant fold hinge rotation during deformation. c) Graph comparing the angle measured on transparencies between the mineral lineation (Lm) and the fold hinge on the upper fold limb (θ_U) and the adjacent lower fold limb (θ_L). The graph shows that $\theta_L > \theta_U$ indicating a combination of both folding and reorientation of Lm around the fold hinge.

layers associated with Stage 1 Initial fold stage and thinner layers Stage 3 Evolved folds. The thinnest layers (mean 3 mm) are typically observed in sheath folds displaying intensely curvilinear ($\delta > 160^\circ$) hinge-lines (Fig. 5). Thicker

quartz mylonite layers also tend to produce longer short limbs on curvilinear folds, perhaps reflecting the control exerted by layer thickness on the wavelength of original buckling (e.g. see Ghosh, 1993 and references therein). However no

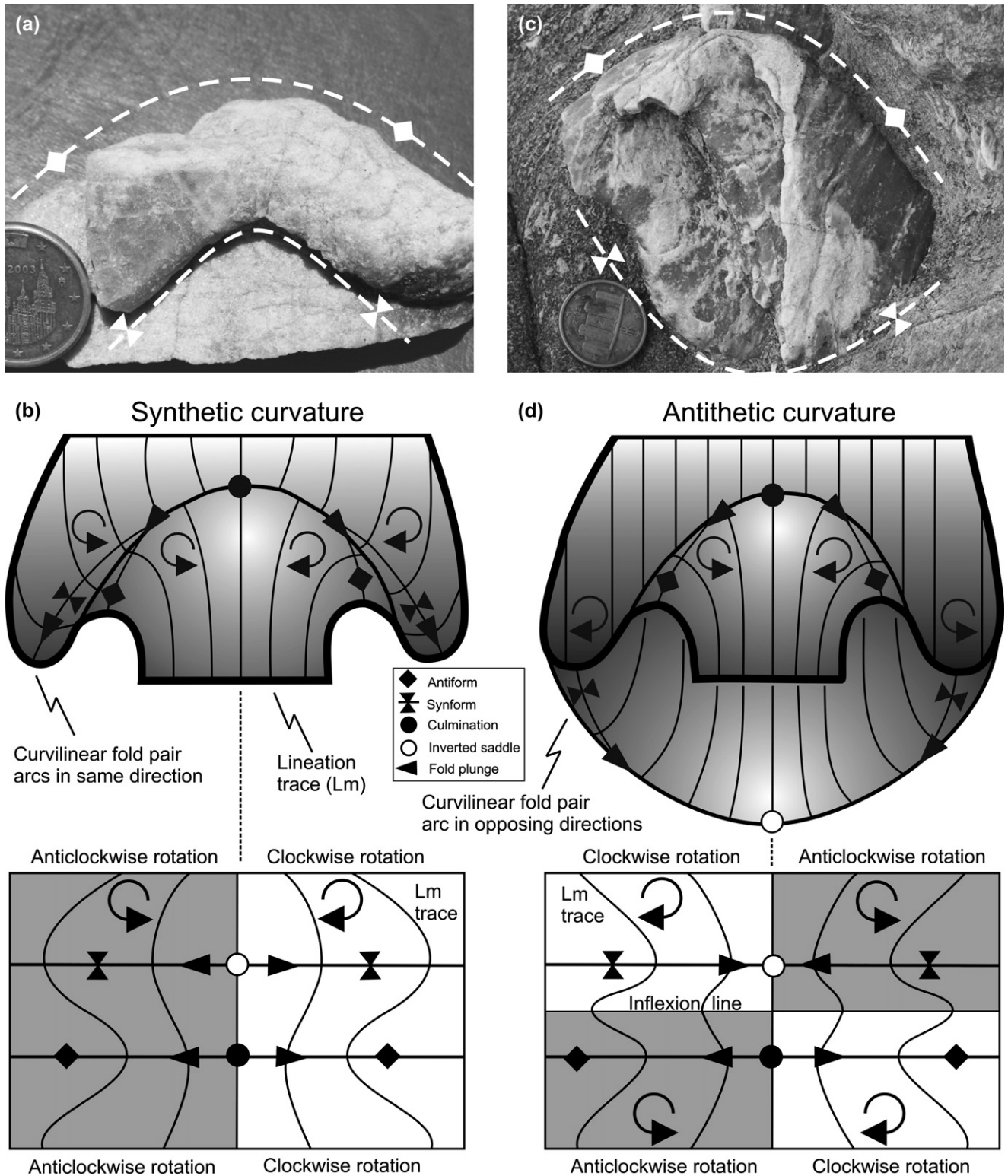


Fig. 10. Photographs and summary 3-D sketches showing a curvilinear antiformal and synformal fold pair displaying the same direction of hinge arcing to define synthetic curvature (a, b) or alternatively opposing senses of curvature to define antithetic curvature (c, d). The unfolded lineation (Lm) pattern is shown directly below in each case.

correlation has been noted between layer thickness and the limb ratio displayed by folds, although limb ratio does decrease with increasing hinge curvilinearity (Fig. 5). This suggests that the short limbs of curvilinear folds are attenuated as

hinge curvature increases to create sheath folds. Similar patterns have been noted on large scale sheaths (e.g. Alsop and Holdsworth, 1999, 2004b; Searle and Alsop, 2007) and models (Cobbold and Quinquis, 1980; Bons and Urai, 1996) and are

consistent with folds developing via stretching of the short limb rather than migrating or rolling hinge models. Our data therefore suggest that original variations in mechanical anisotropy associated with quartz layer thickness pose a significant control on patterns of original “active” buckle folding, and that such geometries may be subsequently amplified and accentuated during “passive” fold evolution associated with progressive shear.

Some of the variation in fabric relationships reflects the hinges of sheath folds displaying components of hinge divergence and bifurcation. Bifurcated hinges are bisected by Lm and display variable (60° – 90°) curvature around the same sheath medial surface. In detail, the curvilinearity of adjacent hinges can vary between 45° and 110° over an interval of just 25 mm (Fig. 8c). This indicates that bifurcation developed prior to hinge rotation (which may have actually enhanced it) and is generated during the initial stages of folding linked to material anisotropy (Fig. 11).

In summary, curvilinear and sheath fold hinges display complex three-dimensional arrangements with one another. This is considered to reflect the irregularity of original fold patterns that are controlled by buckling instabilities and mechanical anisotropy. The range of fold geometries and fabric relationships noted above is perhaps more complex than envisaged in the classic models of Cobbold and Quinquis (1980) (Fig. 11). Patterns of evolving curvilinear folds associated

with initial buckle growth normal to the shear plane have also been described in modelling experiments by Bons and Urai (1996) who note that fold growth can not be simply explained as passive shearing of “initial perturbations” as originally suggested by Quinquis et al. (1978). Our field study demonstrates that folds initiate by buckling of layers, and are then passively amplified to generate the observed range of sheath fold geometries.

6.2. Sheath fold vergence and the transport direction

A common misconception is that sheath fold hinges generated during simple shear-dominated deformation consistently close in the direction of movement and as such can be used to determine bulk shear sense i.e. top-to-the-South shear sense will generate consistently South-closing sheath folds (e.g. Van der Pluijm and Marshak, 2004 p. 314; Davis and Reynolds, 1996 p. 534). Our detailed analysis of sheath folds (e.g. Fig. 7c,d) clearly demonstrates that this is not the case and that sheaths close in *either* sense about the transport direction. Analysis of individual curvilinear fold pairs reveals South-closing folds frequently display greater curvilinearity (mean $\delta = 47^\circ$) when compared to adjacent North-closing return hinges (mean $\delta = 36^\circ$), although axial planes and calculated hinge-girdles display similar obliquities to S_m ($\omega = 24^\circ$). This suggests that folds displayed an original asymmetry, with

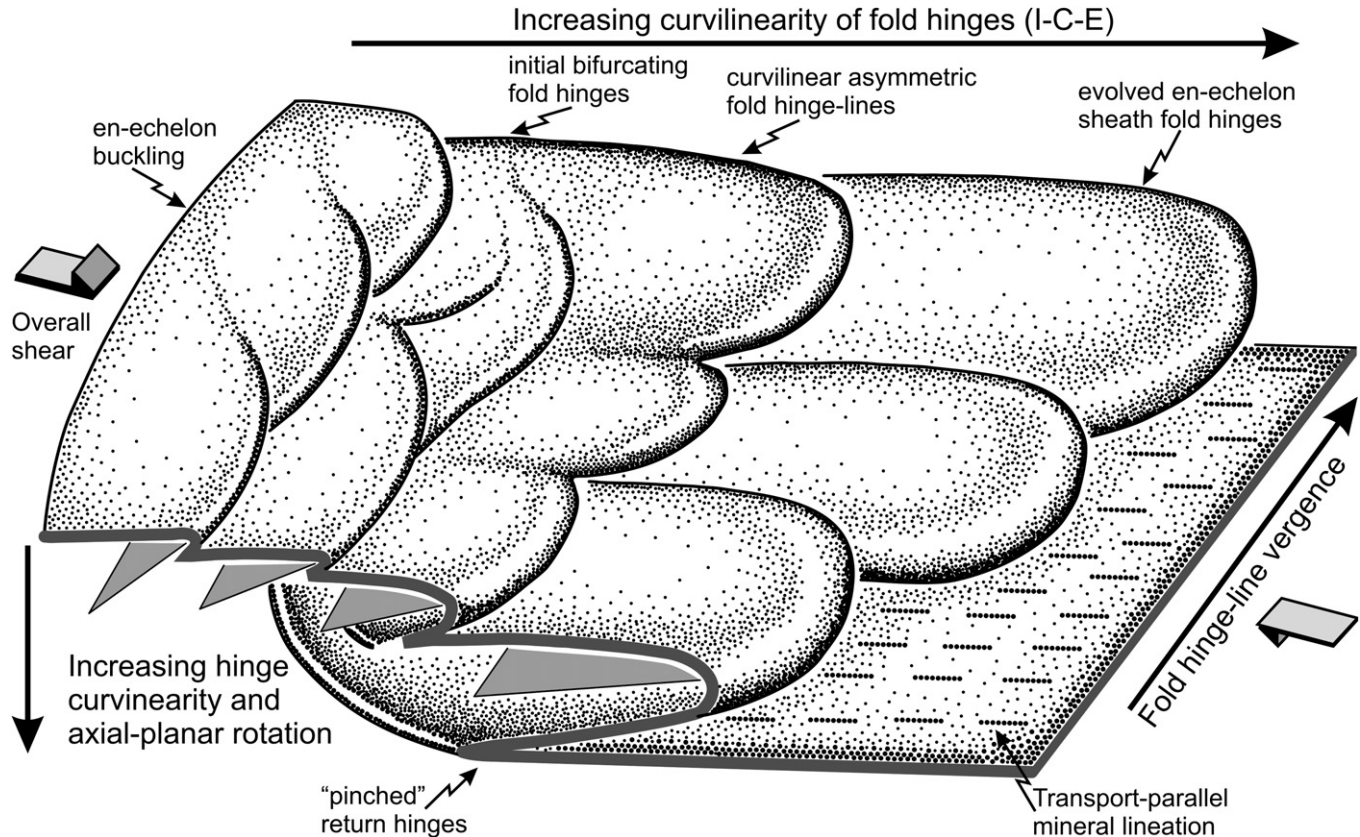


Fig. 11. Summary schematic cartoon illustrating the range of minor fold geometries comprising initial, curvilinear and evolved folds (ICE). Folds display markedly pinched return hinges with an overall sense of fold limb vergence towards the right associated with dextral shear. Fold hinge-line vergence is directed away from the observer.

South closing fold axial planes at greater angles to Sm. South-closing hinges may be better developed and display greater curvilinearity when compared to adjacent (North-closing) return hinges as dextral shear on the NNW trending shear zone will typically generate asymmetric buckles verging towards the South in the direction of shear. Sheath folds closing in a single direction may thus locally dominate over their respective return hinges which become “pinched” due to high shear strains being imposed on original cusped folds (Fig. 8d,e).

Sheath folds closing in the same direction can also display a systematic lateral offset to form a series of closures or “tongues” pointing in the same direction (Fig. 8f). Return hinges may be extremely pinched, such that these “en-echelon sheaths” are apparently positioned directly on top of one another. An overall en-echelon arrangement to sheath folds indicates that each original periclinal buckle was slightly offset from its neighbour. Although not previously described in sheath folds, such an arrangement is frequently observed in periclinal folds (Dubey and Cobbold, 1977; Price and Cosgrove, 1990 p. 265). The en-echelon tongues typically close in the direction of transport and may therefore help determine shear sense (Fig. 11).

Sheath folds in this case study clearly display fold hinge-line vergence towards culmination surfaces (Fig. 8g,h and 11), whilst depression surfaces superimposed on antiformal sheaths are associated with markedly pinched geometries. End member scenarios i.e. domes and basins, may be well-developed, although non-end-member scenarios e.g. saddles, result in pinched and attenuated forms (Fig. 8d,e). Cusped geometries associated with return hinges and fold hinge-line vergence reflect the contrast in competency between quartz mylonite layers and the weaker phyllonitic host during initial buckling. (e.g. Ramsay, 1982; Ramsay and Huber, 1987 p. 394; Price and Cosgrove, 1990 p. 273; Ghosh, 1993 p. 231). Thus, the asymmetry recorded in sheath folds reflects original buckle fold patterns in the shear zone, and may in this case provide a useful guide to shear sense when used in conjunction with other criteria (Fig. 11).

7. Conclusions

a) The establishment of a geometric framework allows a broad threefold division of fold evolution incorporating Initial (0° – 30° hinge curvature), Curvilinear (30° – 90°) and Evolved (90° – 180°) fold stages (I-C-E). The variety of observed fold geometries from sub-cylindrical to intensely curvilinear sheaths simply reflects structures preserved or “frozen” at different stages within ICE along their particular evolutionary route.

b) Increasing angles of fold hinge curvature (δ) are marked by hinge segments rotating into sub-parallelism with Lm, whilst the acute angle between the axial planar hinge girdle and foliation (ω) also displays a sequential reduction. The greatest reduction in ω occurs in the initial fold stage.

c) Mineral lineations (Lm) display curved “U” traces on surfaces which are unfolded about the fold hinge, indicating that the lineation was “active” and recrystallising as the folds developed. Lm typically preserves a larger angle with the fold

hinge on the lower (short) limb (θL) compared to the upper limb ($\theta L > \theta U$). This relationship suggests that θL failed to achieve a new steady orientation and preserves higher values created when the fold hinge was initiated at greater angles to Lm.

d) The sense of “U” shaped curvature displayed by lineations on unfolded surfaces reverses across the nose of sheath folds, reflecting the opposing sense of hinge rotation across sheath culmination and depression surfaces. Curvilinear fold pairs arcing in the same direction will theoretically display *synthetic curvature* with “U” shaped Lm closures pointing in opposing directions along the antiformal and synformal pairs, whilst *antithetic curvature* results in “U” shaped Lm closures pointing in the same direction.

e) Variations in mechanical anisotropy associated with quartz layer thickness can pose a significant control on patterns of original “active” buckle folding, which may be subsequently amplified during “passive” fold evolution associated with progressive shear.

f) Limb ratio decreases with increasing hinge curvilinearity, suggesting that the short limbs of curvilinear folds are attenuated as hinge curvature increases to create sheath folds. Such patterns are consistent with folds developing via stretching of the short limb, rather than migrating or rolling hinge models.

g) Despite many authors showing only one curvilinear hinge in sheath fold pairs, this study unequivocally demonstrates that *both* hinges of fold pairs become curvilinear. The asymmetry recorded in sheath fold pairs, with sheaths closing in the transport direction recording greater hinge-line curvilinearity compared to adjacent return hinges, may reflect original buckle fold patterns. In this case sheath asymmetry can provide a useful guide to shear sense.

Acknowledgements

Fieldwork for this paper was funded by the Carnegie Trust for the Universities of Scotland, together with the Spanish Ministry of Education and Science (project CGL2004-03657/BTE). Both awards are gratefully received. We would also like to thank the two referees for extremely detailed reviews.

References

- Alsop, G.I., Holdsworth, R.E., 1999. Vergence and facing patterns in large-scale sheath folds. *Journal of Structural Geology* 21, 1335–1349.
- Alsop, G.I., Holdsworth, R.E., 2002. The geometry and kinematics of flow perturbation folds. *Tectonophysics* 350, 99–125.
- Alsop, G.I., Holdsworth, R.E., 2004a. Shear zone folds: records of flow perturbation or structural inheritance? In: Alsop, G.I., Holdsworth, R.E., McCaffrey, K.J.W., Hand, M. (Eds.), *Flow Processes in Faults and Shear Zones*. Special Publications, Vol. 224. Geological Society, London, pp. 177–199.
- Alsop, G.I., Holdsworth, R.E., 2004b. The geometry and topology of natural sheath folds: a new tool for structural analysis. *Journal of Structural Geology* 26, 1561–1589.
- Alsop, G.I., Holdsworth, R.E., 2006. Sheath folds as discriminators of bulk strain type. *Journal of Structural Geology* 28, 1588–1606.

- Alsop, G.I., Holdsworth, R.E., 2007. Flow perturbation folding in shear zones. In: Ries, A.C., Butler, R.W.H., Graham, R.D. (Eds.), *Deformation of the Continental Crust: The Legacy of Mike Coward*. Special Publications, Vol. 272. Geological Society, London, pp. 77–103.
- Alsop, G.I., Holdsworth, R.E., McCaffrey, K.J.W., 2007. Scale invariant sheath folds in salt, sediments and shear zones. *Journal of Structural Geology* 29, 1585–1604.
- Bons, P.D., Urai, J.L., 1996. An apparatus to experimentally model the dynamics of ductile shear zones. *Tectonophysics* 256, 145–164.
- Carreras, J., 1997. Shear zones in foliated rocks: geometry and kinematics. In: Sengupta, S. (Ed.), *Evolution of Geological Structures in Micro- to Macro-scales*. Chapman and Hall, London, pp. 185–201.
- Carreras, J., 2001. Zooming on Northern Cap de Creus shear zones. *Journal of Structural Geology* 23, 1457–1486.
- Carreras, J., Casas, J.M., 1987. On folding and shear zone-development: a mesoscale structural study on the transition between two different tectonic styles. *Tectonophysics* 135, 87–98.
- Carreras, J., Garcia-Celma, A., 1982. Quartz c-axis fabric variation at the margins of a shear zone developed in schists from Cap de Creus (Spain). *Acta Geologica Hispanica* 17, 137–149.
- Carreras, J., Santanach, P.F., 1973. Micropliegues y movimiento en los cisalamientos profundos del Cabo de Creus (prov. De Gerona, Espana). *Estudios Geologicos* 29, 439–450.
- Carreras, J., Estrada, A., White, S., 1977. The effects of folding on the C-axis fabrics of a quartz mylonite. *Tectonophysics* 39, 3–24.
- Carreras, J., Druguet, E., Gria, A., 2005. Shear zone-related folds. *Journal of Structural Geology* 27, 1229–1251.
- Cobbold, P.R., Quinquis, H., 1980. Development of sheath folds in shear regimes. *Journal of Structural Geology* 2, 119–126.
- Davis, G.H., Reynolds, S.J., 1996. *Structural Geology of Rocks and Regions*, 2nd ed. Wiley, New York.
- Dubey, A.K., Cobbold, P.R., 1977. Noncylindrical flexural slip folds in nature and experiment. *Tectonophysics* 38, 223–239.
- Fossen, H., Rykkelid, E., 1990. Shear zone structures in the Øygarden area, West Norway. *Tectonophysics* 174, 385–397.
- Ghosh, S.K., 1993. *Structural Geology: Fundamentals and Modern Developments*. Pergamon Press, 598 pp.
- Ghosh, S.K., Chatterjee, A., 1985. Patterns of deformed early lineations over later folds formed by buckling and flattening. *Journal of Structural Geology* 7, 651–666.
- Ghosh, S.K., Sengupta, S., 1984. Successive development of plane noncylindrical folds in progressive deformation. *Journal of Structural Geology* 6, 703–709.
- Ghosh, S.K., Sengupta, S., 1987. Progressive development of structures in a ductile shear zone. *Journal of Structural Geology* 9, 277–287.
- Ghosh, S.K., Hazra, S., Sengupta, S., 1999. Planar, non-planar and refolded sheath folds in the Phulad Shear Zone, Rajasthan, India. *Journal of Structural Geology* 21, 1715–1729.
- Jiang, D.Z., Williams, P.F., 1999. When do drag folds not develop into sheath folds in shear zones? *Journal of Structural Geology* 21, 577–583.
- Kuiper, Y.D., Jiang, D., Lin, S., 2007. Relationship between non-cylindrical fold geometry and the shear direction in monoclinic and triclinic shear zones. *Journal of Structural Geology* 29, 1022–1033.
- Mandal, N., Samanta, S.K., Chakraborty, C., 2004. Problem of folding in ductile shear zones: a theoretical and experimental investigation. *Journal of Structural Geology* 26, 475–489.
- Marques, F.G., Cobbold, P.R., 1995. Development of highly non-cylindrical folds around rigid ellipsoidal inclusions in bulk simple shear regimes: natural examples and experimental modeling. *Journal of Structural Geology* 17, 589–602.
- Passchier, C.W., 1997. The fabric attractor. *Journal of Structural Geology* 19, 113–127.
- Passchier, C.W., Trouw, R.A.J., 2005. *Microtectonics*, 2nd ed. Springer, 366 pp.
- Passchier, C.W., den Brok, S.W.J., van Gool, J.A.M., Marker, M., Manatschal, G., 1997. A laterally constricted shear zone system – the Nordre Strømfjord steep belt. *Nagssugtoqidian Orogen, W. Greenland*. *Terra Nova* 9, 199–202.
- Price, N.J., Cosgrove, J.W., 1990. *Analysis of Geological Structures*. Cambridge University Press, 502 pp.
- Quinquis, H., Audren, C., Brun, J.P., Cobbold, P., 1978. Intensive progressive shear in Ile de Groix blueschists and compatibility with subduction or obduction. *Nature* 274, 43–45.
- Ramsay, J.G., 1980. Shear zone geometry: a review. *Journal of Structural Geology* 2, 83–99.
- Ramsay, J.G., 1982. Rock ductility and its influence on the development of tectonic structures in mountain belts. In: Hsu, K.J. (Ed.), *Mountain Building Processes*. Academic Press, pp. 111–127.
- Ramsay, J.G., Huber, M.I., 1987. *The Techniques of Modern Structural Geology. Folds and Fractures*, Vol. 2. Academic Press.
- Rosas, F., Marques, F.O., Luz, A., Coelho, S., 2002. Sheath folds formed by drag induced by rotation of rigid inclusions in viscous simple shear flow: nature and experiment. *Journal of Structural Geology* 24, 45–55.
- Searle, M.P., Alsop, G.I., 2007. Eye to eye with a mega-scale sheath fold: a case study from Wadi Mayh, northern Oman Mountains. *Geology* 35, 1043–1046.
- Sengupta, S., Ghosh, S.K., 1997. The kinematic history of the Singhbhum Shear Zone. *Proceedings of the Indian Academy of Sciences (Earth and Planetary Sciences)* 106, 185–196.
- Sengupta, S., Ghosh, S.K., 2004. Analysis of transpressional deformation from geometrical evolution of mesoscopic structures from Phulad shear zone, Rajasthan, India. *Journal of Structural Geology* 26, 1961–1976.
- Sengupta, S., Ghosh, S.K., 2007. Origin of striping lineation and transposition of linear structures in shear zones. *Journal of Structural Geology* 29, 273–287.
- Sengupta, S., Koyi, H.A., 2001. Modifications of early lineations during later folding in simple shear. In: Koyi, H.A., Mancktelow, N.S. (Eds.), *Tectonic Modeling: A Volume in Honour of Hans Ramberg*, Vol. 193. Geological Society of America Memoir, Boulder, Colorado, pp. 51–68.
- Skjerna, L., 1989. Tubular folds and sheath folds: definitions and conceptual models for their development, with examples from the Grapesvare area, northern Sweden. *Journal of Structural Geology* 11, 689–703.
- Srivastava, D.C., 2001. Deformation pattern in the Precambrian basement around Masuda, Central Rajasthan. *Journal of the Geological Society of India* 57, 197–222.
- Van der Pluijm, B.A., Marshak, S., 2004. *Earth Structure: An Introduction to Structural Geology and Tectonics*, 2nd ed. W.W. Norton and company, New York.
- Williams, P.F., Jiang, D., Lin, S., 2006. Interpretation of deformation fabrics of infrastructure zone rocks in the context of channel flow and other tectonic models. In: Law, R.D., Searle, M.P., Godin, L. (Eds.), *Channel Flow, Ductile Extrusion and Exhumation in Continental Collision Zones*. Special Publications, Vol. 268. Geological Society, London, pp. 221–235.